Surfaces, Interfaces, and Applications

# Synergy between Silver-Copper Surface Alloy Composition and Carbon Dioxide Adsorption and Activation

Yifan Ye, Jin Qian, Hao Yang, Hongyang Su, Kyung-Jae Lee, Ane Etxebarria, Tao Cheng, Hai Xiao, Junko Yano, William A. Goddard, and Ethan J. Crumlin

*ACS Appl. Mater. Interfaces*, **Just Accepted Manuscript** • DOI: 10.1021/acsami.0c02057 • Publication Date (Web): 08 May 2020

# Synergy between Silver-Copper Surface Alloy Composition and Carbon Dioxide Adsorption and Activation

Yifan Ye[1,2,3,#], Jin Qian[3,4,#], Hao Yang[4,5#], Hongyang Su[2,6], Kyung-Jae Lee[2,7], Ane Etxebarria[2,8,9], Tao Cheng[4,5,10], Hai Xiao[4,10], Junko Yano[1,11*], William A. Goddard III[4,10*], Ethan J. Crumlin[2,3*]

[1] Joint Center for Artificial Photosynthesis, Lawrence Berkeley National Laboratory, Berkeley, CA 94720, United States;

[2] Advanced Light Source, Lawrence Berkeley National Laboratory, Berkeley, CA 94720, United States;

[3] Chemical Sciences Division, Lawrence Berkeley National Laboratory, Berkeley, CA 94720, United States;

[4] Materials and Process Simulation Center, California Institute of Technology, Pasadena, CA 91125, United States;

[5] Institute of Functional Nano&Soft Materials (FUNSOM), Jiangsu Key Laboratory for Carbon-Based Functional Materials & Devices, Soochow University, Jiangsu, 215123, China;

[6] Hefei National Laboratory for Physical Sciences at the Microscale, University of Science and Technology of China, Hefei, Anhui 230026, P. R. China;

[7] Department of Physics and Photon Science, Gwangju Institute of Science and Technology (GIST), Gwangju 500-712, South Korea;

[8] Centre for Cooperative Research on Alternative Energies (CIC energiGUNE), Basque Research and Technology Alliance (BRTA), Alava Technology Park, Albert Einstein 48, 01510 Vitoria-Gasteiz, Spain;

[9] Department of Condensed Matter Physics, Faculty of Science and Technology, University of the Basque Country, UPV/EHU, Apdo 644, 48080 Bilbao, Spain;

[10] Joint Center for Artificial Photosynthesis, California Institute of Technology, Pasadena CA 91125, United States;

[11] Molecular Biophysics and Integrated Bioimaging Division, Lawrence Berkeley National Laboratory, Berkeley, CA 94720, United States.

# These authors contributed equally

***Corresponding Authors:** jyano@lbl.gov; wag@caltech.edu; ejcrumlin@lbl.gov

**Abstract**

Bimetallic electrocatalysts provide a promising strategy for improving performance, especially in the enhancement of selectivity of $CO_2$ reduction reactions. However, the first step of $CO_2$ activation on bimetallic materials remains obscure. Considering bimetallic silver-copper (AgCu) as an example, we coupled ambient pressure X-ray photoelectron spectroscopy (APXPS) and quantum mechanics (QMs) to examine $CO_2$ adsorption and activation on AgCu exposed to $CO_2$ with and without $H_2O$ at 298 K. The interplay between adsorbed species and the surface alloy composition of Cu and Ag is studied in atomic details. The APXPS experiment as well as DFT calculations indicate that the clean sample has an Ag rich surface layer. Upon adsorption of $CO_2$ and surface O, we found that it is thermodynamically more favorable to induce subsurface Cu to substitute for some surface Ag atoms, modifying the stability and activation of $CO_2$ related chemisorbed species. We further characterized this substitution effect by correlating the new adsorption species with the observed binding energy shift and intensity change in APXPS.

**Keywords**

$CO_2$ adsorption; $CO_2$ activation; Surface reconstruction; Density Functional Theory (DFT); Ambient Pressure XPS (APXPS)

## 1. Introduction

Converting carbon dioxide ($CO_2$) into liquid fuels and feedstock chemicals is an attractive approach to close the anthropogenic carbon cycle while creating new energy cycles for storing renewable energy in the form of hydrocarbon-based energy-dense fuels.[1-5] Advanced electrocatalysts are required to convert inert $CO_2$ to various hydrocarbon-based chemicals.[6-7] An emerging design principle is to utilize multicomponent materials to promote the $CO_2$ reduction reaction ($CO_2RR$). Typically in a bimetal system, one metal has high selectivity for producing CO (such as Ag and Au)[8-13], while the other metal is Cu, [13-16] the only metal that has been shown to reduce CO to multi-carbon products.[17] Recently, the silver-copper (AgCu) catalyst has demonstrated a dramatic improvement in product selectivity and activity compared to pure Cu catalyst.[18-21] However, the bimetal systems underlying $CO_2RR$ activation mechanism responsible for the enhanced catalytic performance remains unclear. Various reaction mechanisms have been suggested based on preconceived notions of the material properties and reaction mechanisms. To optimize such alloy systems, it is essential to develop a comprehensive atomistic level understanding of how $CO_2$ is activated by alloy catalyst surfaces.

$CO_2RR$ is complex, involving applied potential, ions in the electrolyte, pH value of the electrolyte and many other factors. Given this complexity, we wanted to decouple this catalytic process into $CO_2$ adsorption/activation (presumably gas-phase dominated), and sequential reaction steps (presumably dominated by electrochemical conditions). In this work, we aim to understand the first steps of $CO_2$ adsorption/activation on AgCu bimetallic surface, focusing on fundamental questions regarding identification of the active species/sites, the functionality of each metal sites, and the catalyst structural evolution that remain unexamined.

We previously explored the dramatically different $CO_2$ adsorption and activation behaviors observed on pure Cu and Ag surfaces at 298 K.[22-24] On a Cu surface, gaseous $CO_2$ ($g$-$CO_2$) is stabilized on the surface as physisorbed linear $CO_2$ ($l$-$CO_2$), and then converted to chemisorbed bent $CO_2$ ($b$-$CO_2$) by forming hydrogen bonds (HBs) with surface adsorbed $H_2O$.[22-23] In contrast, on an Ag surface, $g$-$CO_2$ reacts with surface O to form a chemisorbed surface species ($O{=}CO_2^{\delta-}$), which stabilizes up to four water molecules through HBs with $O{=}CO_2^{\delta-}$. In addition, chemisorbed $b$-$CO_2$ is also stabilized on the Ag by HBs from two waters.[24] These dramatic differences of $CO_2$ interacting with Ag or Cu surfaces motivates this study, to understand how $CO_2$ interacts with the AgCu surface alloy.

In this work, we combined *in-situ* ambient pressure X-ray photoelectron spectroscopy (APXPS) with quantum mechanics (QM) to obtain a comprehensive understanding of how $CO_2$ and $H_2O$ interact with the

AgCu surface to initiate $CO_2$ adsorption and activation. Our findings are summarized in **Figure 1**. We found both $O{=}CO_2^{\delta-}$ and *l*-$CO_2$ are stable on the AgCu surface exposed solely to 0.3 Torr $CO_2$. On the other hand, $(O{=}CO_2^{\delta-})$-$(H_2O)_{1\text{-}4}$ and (*b*-$CO_2$)-$(H_2O)_2$ form on AgCu when 0.15 Torr $H_2O$ is combined with 0.3 Torr $CO_2$. Due to the interplay between Ag and Cu at the surface, adsorbates on AgCu have different geometrical and electronic structures as exhibited in the C 1s binding energy (BE) shifts compared to those on pure Ag and Cu. We also observed that chemistry driven surface reconstruction for the AgCu bimetallic system, induced by surface adsorption, changes the Ag and Cu distribution on the surface as well as the $CO_2$ surface adsorption configuration. We observed the formation of surface O when these systems are exposed to $CO_2$ or $H_2O$, which may arise from dissociative reactions on the Ag sites. We observed that this surface O then attracts subsurface Cu to the surface, promoting Cu substitution of Ag in the surface layer. This chemistry driven surface reconstruction process is shown in **Figure 2** and **3**. A small amount of surface O is involved in the surface reconstruction. However, the current AgCu system differs from the extensively reported metal-metal oxide systems.[25-31] The bimetallic surface exhibits a synergetic effect between the Ag and Cu surface composition that tunes the $CO_2$ ($H_2O$)-AgCu interactions, initiating surface reconstruction, and altering the $CO_2$ activation process. Thus, $CO_2$ adsorption and activation on AgCu surfaces operates entirely differently compared to pure Ag or Cu surface, providing possibilities for further tuning $CO_2$ adsorption behavior to facilitate selective product formation.

## 2. Methods:

### 2.1 Sample preparation:

The AgCu bimetal samples were made by a physical melting method. First, Ag (99.999%) and Cu (99.999%) were melted in the atomic ratio of 1:4 under argon (Ar) in a vacuum arc furnace; following, the molten mixtures were quenching in the deionized (DI) water and cold-rolled into foils; lastly, the foils were polished with sandpapers (600, 1200, and 2500 grit 3M) and cleaned with DI water and Ethanol. The samples showed (111) surface orientation after treatment.[21] The samples were cut to size of 8 × 8 $mm^2$ to fit the sample holder and transferred to a vacuum chamber with base pressure of $8\times10^{-10}$ Torr at beamline 9.3.2 at Advanced Light Source (ALS), Lawrence Berkeley National Laboratory (LBNL). The sample surface was cleaned by repeated Ar sputtering and rapid low temperature thermal annealing. Ar sputtering was performed using $8\times10^{-6}$ Torr Ar gas (2 kV, 20 mA) for 1hour in the first 2 cycles. The thermal treatment was performed by increasing the temperature rapid to ~400 K, holding the temperature for 5 mins, and then cooling down the sample to room temperature in the first 2 cycles. For the last treatment cycle, a mild Ar sputtering was performed (1.5 kV, 10 mA) for 30 mins, while a rapid thermal treatment was done by increasing the temperature to ~350 K, holding the temperature for 1 min, and then cooling down the sample

to room temperature. With these surface treatments, the surface condition can be restored regardless of the initial surface conditions. Staring from this initial surface, the AgCu sample was heated at 450 K for 5 mins to get an Ag-rich surface. We denoted the initial- and heat-treated sample as Ag-lean and Ag-rich AgCu samples, respectively.

**2.2 APXPS measurements:**

Ambient pressure XPS measurements were performed at beamline 9.3.2 of the ALS, LBNL.[32] The samples were cleaned in the preparation chamber of the beamline and transferred to the main chamber for further characterization and *in-situ* gas adsorption experiments. The APXPS spectra were collected in the following order: a low-resolution survey scan with a binding energy of 600 eV to –5 eV at photon energy of 670 eV, then high-resolution scans of O 1s, C 1s, Ag 3d and Cu 3p at different photon energies. For each condition, samples were equilibrated for at least 30 mins before the measurement. The C 1s and O 1s signals representing the surface adsorbates properties were taken with photon energies of 415 eV and 670 eV, respectively, to get a surface sensitive probe with the photoelectron kinetic energy of ~130 eV. Due to the beamline limitation, we cannot take Cu 3p (and/or Cu 2p) spectra with 130 eV photoelectron kinetic energy. Thus, we used 670 eV and 800 eV, and 380 eV and 510 eV photon energies to monitor the Ag 3d and Cu 3p signals at surface and bulk, respectively. The catalyst components distribution at the surface was quantified using the same kinetic energies probe by first normalizing the raw signals to the beam flux and then applying the cross-section factors. By taking spectra at different sample spots and comparing spectra before and after beam illumination for 2 hours, we found beam damage on the sample is negligible during the measurements.

The gas adsorption experiments were performed at 298 K with APXPS recorded. The $CO_2$ partial pressure was kept at 0.3 Torr for $CO_2$ adsorption, whereas the total pressure was kept at 0.45 Torr with 0.3 Torr $CO_2$ and 0.15 Torr $H_2O$. The $H_2O$ was degassed using the freeze-pump-thaw method for three cycles to ensure no dissolved gases. All the gas-lines were well cleaned and baked before dosing gases. The dosing gas ($CO_2$, $H_2O$) purities were *in-situ* monitored by a conventional quadrupole mass spectrometer to ensure no additional gas cross-contamination (especially, the CO and $H_2$ gases).

**2.3 QM predictions:**

Since the AgCu samples were made through high temperature treatments, we expect that the surface prefers the (111) surface for both fcc metals, as established experimentally.[21] Thus, the QM studies assume the (111) surface, which we describe using a 4 × 4 supercell. We include 4 (111) layers in which the bottom 2 are fixed. We left 15 Å in the z direction to avoid interaction between periodic cells. The convergence test

with 4-7 layers and vacuum region of 10 Å were conducted and the results are shown in **Table S1**. The top two layers were relaxed, and the bottom layers were fixed during the optimization. We found that all structures of adsorbed $O{=}CO_2^{\delta-}$ species are maintained, and the adsorption energy is on average −0.74 eV (*E*) and −0.27 eV (*G*), which is very close to the values that we obtained assuming the 4-layer structures. The 4-layer model is sufficiently reliable to represent the properties of these periodic systems.

All calculations were carried out with the Vienna *Ab-initio* Simulation Package (VASP).[33] We used the Perdew–Burke–Ernzerhof (PBE) formulation of the generalized gradient approximation (GGA) exchange-correlation functional using the projector-augmented (PAW) method and including the D3 (Grimme, Becke, and Johnson) empirical corrections for long-range London dispersion.[34-36] A plane-wave basis set cutoff of 600 eV and an energy smearing of 0.2 eV using the first order Methfessel–Paxton scheme were employed.[37] The electron self-consistent calculations are considered to be converged when the energy differences are less than $10^{-6}$ eV. The structure optimizations are considered converged when force differences are less than $10^{-4}$ eV Å$^{-1}$. Reciprocal space was sampled by a Γ-centered Monkhorst-Pack 3 × 3 × 1 scheme for all calculations. More details can be found in the previous study[24] and in the supporting information.

## 3. Results

### 3.1 Clean AgCu surface with no adsorbates

Using APXPS we examined two different AgCu surface ratios under vacuum at 298 K prior to $CO_2$ adsorption. From the spectra we know that there is no inner charge transfer between Ag and Cu in AgCu (**Figure S1**).[21, 38] Quantified by APXPS under vacuum at 298 K, the Ag-lean samples have Ag:Cu ratio of 0.2:1 while the Ag-rich samples have 0.7:1, over the top ~2.4 nm layer, becoming 0.1:1 and 0.3:1, respectively, over the top ~3.6 nm layer (**Figure S1**). This enrichment of Ag at the surface indicates that Ag atoms prefer the surface compared to bulk in the AgCu matrix under vacuum, which is expected from the low surface energy of Ag (1250 mJ/m$^2$) compared to Cu (1830 mJ/m$^2$).[39] Our QM predictions also found it 0.18 eV more favorable for Cu to be doped in the bulk compared to the surface (**Figure S2**) under vacuum at 298 K, justifying our simulation model which started with pure Ag in the outer most surface layer. This is further verified by heating the AgCu sample, which results in Ag migration to the surface (**Figure S1** and **Figure S3**).

### 3.2 $CO_2$ adsorption on AgCu surfaces

We first determined which species are stable on Ag and Cu exposed to $CO_2$, namely $O{=}CO_2^{\delta-}$ on Ag and *l*-$CO_2$ on Cu,[22, 24] and we evaluated their stabilities on the new bimetallic AgCu surface, while gradually

doping more and more surface Cu atoms into the Ag surface. We reported earlier that $CO_2$ adsorbs on Ag surface to form $O{=}CO_2^{\delta-}$ with two O atoms on the surface interacting with five Ag atoms and the C=O double bond pointing away from the surface. Our QM predictions found that replacing Ag atoms with Cu atoms modifies the surface $O{=}CO_2^{\delta-}$ properties. Since one surface O can attract up to three Cu atoms to the surface (**Figure S4**), we considered the systematic substitution of three Ag atoms with Cu underneath a surface O. The only stable $O{=}CO_2^{\delta-}$ configuration on the AgCu matrix has one Cu replacing the Ag atom under the C atom, leading to $E_{ads} = -0.55$ eV and $\Delta G = -0.08$ eV (**Figure 1a**), while having one Cu under the O atom or having two or three Cu atoms substituted for Ag in the surface destabilize $O{=}CO_2^{\delta-}$. With $O{=}CO_2^{\delta-}$ on the AgCu surface, it interacts closely with five catalyst atoms (**Figure S5**). Thus, we denote this stable configuration as $(O{=}CO_2^{\delta-})$-(4Ag1Cu).

We found that $(O{=}CO_2^{\delta-})$-(4Ag1Cu) has a $C{=}O_{up}$ double bond (with a length of 1.22 Å) pointing up normal to the surface while the other two O bind to two-Ag and one-Cu with C-O lengths of 1.36 Å, similar to that on Ag. We observed that $(O{=}CO_2^{\delta-})$-(4Ag1Cu) has two O-Ag distances of 2.43 Å and 2.39 Å while the O-Cu distance is 2.12 Å. Those distances are smaller than on pure Ag which exhibited three O-Ag distances of 2.65 Å, 2.38 Å, and 2.28 Å. The slightly modified geometry leads to a change in the charge distribution on the $O{=}CO_2^{\delta-}$ compared to that on Ag. Bader charge analyses[40-41] showed that the total charge of $O{=}CO_2^{\delta-}$ on AgCu is −1.16e with a C charge of +1.53e, compared to a total charge of −1.26e and carbon charge of +1.47e on the pure Ag(111) surface. The increased positive charge on the C atom leads to a predicted C 1s binding energy (BE) +0.34 eV higher than that for the Ag surface, leading to a predicted experimental C 1s BE of 288.2 eV compared to 287.9 eV on pure Ag surface (**Figure 1b,c**). We also tested the stability of $O{=}CO_2^{\delta-}$ on AgCu with Cu at the 2nd and 3rd layer (**Table S2**). We found that Cu atoms prefer to stay on the surface when adsorbents such as O and $O{=}CO_2^{\delta-}$ are present. Having Cu atoms buried inside the Ag matrix does not affect the adsorption geometry nor XPS binding energy.

For *l*-$CO_2$, our QM predictions found that at least two surface Cu atoms combined with a subsurface O is required to stabilize *l*-$CO_2$ on the AgCu surface. Since the surface prefers to have Ag, a surface O is required to bring these two Cu atoms to the surface (**Figure S2**). Thus, we denoted this stable configuration as (*l*-$CO_2$)-(2Ag2Cu1$O_{surf}$1$O_{sub}$) (**Figure S5**). With surface O and two adjacent Cu atoms in the Ag matrix, we found that *l*-$CO_2$ prefers to be perpendicular to the Cu pair (**Figure 1a**), rather than parallel (**Figure S6**). This stable configuration is 3.32 Å above the surface with $E_{ads} = -0.54$ eV, $\Delta G = -0.06$ eV. The predicted C 1s BE is +0.2 eV higher than *l*-$CO_2$ on Cu, which is found experimentally to be at 288.6 eV (**Figure 1b,c**).

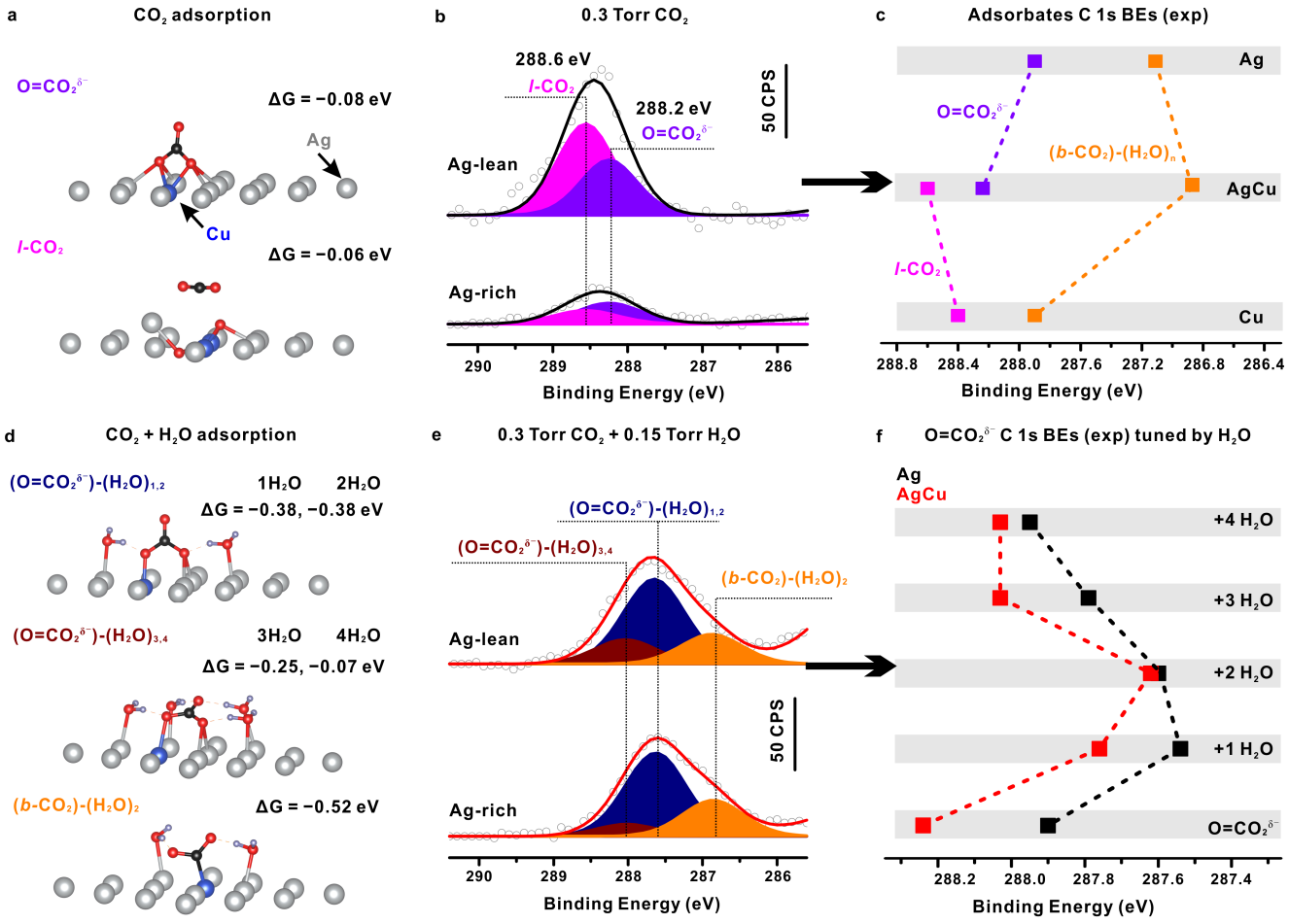


**Figure 1. The QM predictions and experimental observations of AgCu surface with $CO_2$ adsorption alone and in the presence of $H_2O$ at 298 K. (a)** Predicted structures for adsorbates, $O{=}CO_2^{\delta-}$ and *l*-$CO_2$, on AgCu surface exposed to 0.3 Torr $CO_2$. **(b)** The C 1s APXPS spectra for adsorbates on AgCu surfaces in the presence of 0.3 Torr $CO_2$ at 298 K. To deconvolute the experimental peak we assume that the two C 1s peaks arising from $O{=}CO_2^{\delta-}$ and *l*-$CO_2$ are separated by 0.4 eV as found with QM predictions. **(c)** The experimental C 1s BEs of various adsorbates on Ag, Cu, and AgCu surfaces. The adsorbate BEs change for different surfaces shows the tunability of adsorbates properties from altered gas-catalyst interaction. **(d)** Predicted structures for adsorbates, $(O{=}CO_2^{\delta-})$-$(H_2O)_{1\text{-}4}$ and (*b*-$CO_2$)-$(H_2O)_2$, on AgCu surface exposed to 0.3 Torr $CO_2$ and 0.15 Torr $H_2O$. The adsorbed $O{=}CO_2^{\delta-}$ species stabilizes one or two $H_2O_{ad}$ via HBs to the O on surface and two more water with HBs to the C=O. The *b*-$CO_2$ becomes stabilized by a pair of $H_2O_{ad}$ each forming a HB with an O of *b*-$CO_2$. **(e)** The C 1s APXPS spectra for adsorbates on AgCu surfaces in the presence of 0.3 Torr $CO_2$ and 0.15 Torr $H_2O$ at 298 K. The peak separations used for this deconvolution were determined from the theory. **(f)** The experimental C 1s BE changes for $O{=}CO_2^{\delta-}$ without and with 1 to 4 $H_2O$ on Ag and AgCu surfaces.

The C 1s spectra of AgCu surfaces exposed to $CO_2$ showed a spectral shape similar to those on Ag but not on Cu (**Figure 1b,** and **Figure S7**).[22, 24] The adsorbate peak in the region from 286 eV to 290 eV shifted

and broadened significantly compared to pure Cu or Ag.[24,27] The full width at half maximum (FWHM) on AgCu is ~1.2 eV, significantly larger than ~0.8 eV obtained on Ag surfaces, indicating more than one adsorbate resides on the AgCu surface after exposure to $CO_2$.

Using the ΔBE predicted from the QM, we de-convoluted the C 1s spectra of the AgCu surface into two peaks: $O{=}CO_2^{\delta-}$ at 288.2 eV and *l*-$CO_2$ at 288.6 eV (**Figure 1b**). We calculated the ratio of ($O{=}CO_2^{\delta-}$)-(4Ag1Cu) to (*l*-$CO_2$)-(2Ag2Cu1$O_{surf}$) to be ~1.5:1 on Ag-rich and ~0.6:1 on Ag-lean surfaces. The larger population of ($O{=}CO_2^{\delta-}$)-(4Ag1Cu) than (*l*-$CO_2$)-(2Ag2Cu1$O_{surf}$) on Ag-rich surfaces is consistent with that $O{=}CO_2^{\delta-}$ and *l*-$CO_2$ dominating the adsorption of $CO_2$ on Ag and Cu, respectively. The change of $O{=}CO_2^{\delta-}$ and *l*-$CO_2$ populations on surfaces with different AgCu compositions (**Figure 1b**) and the shifts in C 1s BEs with respect to pure Ag and Cu (**Figure 1c**) demonstrate the tunability of the surface alloy composition to the surface adsorbates.

### 3.3 $CO_2$ adsorption on AgCu surfaces modified by surface $H_2O$

We next evaluated the $CO_2$ adsorption in the presence of $H_2O$ on AgCu surfaces. QM found that surface $H_2O$ makes HBs both to chemisorbed $O{=}CO_2^{\delta-}$ and to physisorbed *l*-$CO_2$ on AgCu. On AgCu, $O{=}CO_2^{\delta-}$ stabilizes up to four $H_2O$, with the first two $H_2O$ forming HBs to each O bonded to the surface, and the 3$^{rd}$ and 4$^{th}$ $H_2O$ making HBs to the two $sp^2$ lone pairs on the C=O unit (**Figure 1d**). On AgCu, the attachment of successive *n*$H_2O$ (*n* = 1 – 4) to $O{=}CO_2^{\delta-}$ leads to ΔG= −0.38 eV, −0.38 eV, −0.25 eV, and −0.07 eV, respectively. The first two $H_2O$ bonding to the O linkage to Ag lead to little change in the geometry, while the 3$^{rd}$ and 4$^{th}$ $H_2O$ force the C=O bond to rotate from being perpendicular to the surface to tilting nearly parallel to the surface. The QM predicted C 1s BEs are 269.31 eV, 269.17 eV, 269.58 eV, and 269.56 eV, respectively. It is worth noting that QM predicts the ΔBE rather than the absolute BE, therefore to convert QM predicted BE to values that are experimentally observed (**Figure 1f**), a rigid shift of ~18.5 eV should be added. Moreover, starting with the different C 1s BEs of $O{=}CO_2^{\delta-}$ on Ag and AgCu, we found that attaching two $H_2O$ or four $H_2O$ onto the $O{=}CO_2^{\delta-}$ lead to almost the same BEs on both surfaces (**Figure 1f**), indicating that surface $H_2O$ may help balance and redistribute the surface adsorbate charge to reach a stable state. The energetics clearly show the tunability of the surface adsorbate properties, and how they can be easily modified by surface $H_2O$.

On both pure Ag and Cu surfaces, we observed that surface water stabilizes the *b*-$CO_2$. The same behavior occurred on the AgCu surface, with *b*-$CO_2$ stabilized by forming HBs with two waters, where two $H_2O$ are on Ag sites and the carbon of *b*-$CO_2$ is on the Cu site. The (*b*-$CO_2$)-$(H_2O)_2$ on the Ag matrix with 1Cu substituted has ΔG = −0.52 eV (**Figure 1d**) and a QM C 1s BE = −268.42 eV.

Using the QM predicted ΔBE, we were able to resolve the experimental peaks for the $(O{=}CO_2^{\delta-})$-$(H_2O)_{1\text{-}4}$ and ($b$-$CO_2$)-$(H_2O)_2$ on AgCu, leading to 287.76 eV, 287.62 eV, 288.03 eV and 288.03 eV, and 286.87 eV, respectively. Accordingly, we used three components, $(O{=}CO_2^{\delta-})$-$(H_2O)_{1,2}$ (with an indistinguishable BE difference of 0.1 eV), $(O{=}CO_2^{\delta-})$-$(H_2O)_{3,4}$, and ($b$-$CO_2$)-$(H_2O)_2$, to de-convolute the adsorbate peak. The spectral fitting results show that the surface is dominated by $(O{=}CO_2^{\delta-})$-$(H_2O)_{1,2}$ and ($b$-$CO_2$)-$(H_2O)_2$. We obtained a higher population of ($b$-$CO_2$)-$(H_2O)_2$ on AgCu surface compared to that on Ag surface, indicating the change of the surface chemistry, which is consistent with Cu promoting the formation of $b$-$CO_2$.[22-23, 42] This strong agreement between the QM predictions and experimental observations validates the accuracy of the surface adsorbate assignments.

### 3.4 Surface reconstruction induced by $CO_2$ adsorption and further altered gas adsorption

Experimentally, we have observed $(O{=}CO_2^{\delta-})$–(5Ag) at 287.9 eV on pure Ag, but we do not find such a peak on the AgCu alloy surface (**Figure 1b**). This discrepancy is explained by the surface substitution of subsurface Cu to surface Ag upon the adsorption of gases species. We find that $CO_2$ adsorption induces a transformation of the AgCu surface configuration (**Figure 2**). For pristine AgCu samples with no gas adsorption (essentially under ultra-high vacuum), Ag is 0.18 eV more favorable to stay at the outermost surface layer than Cu (**Figure S2**). Since surface O is required to form $O{=}CO_2^{\delta-}$ on the surface, we calculated the thermodynamics driving forces controlling how a surface O forms on the outmost Ag layer and how the AgCu surface reconstruction is initiated. For the AgCu surface with adsorbed $O{=}CO_2^{\delta-}$, we consider the changes of the top two layers and the 5 atoms that interact closely with $O{=}CO_2^{\delta-}$ (**Figure 2a**). With O and $CO_2$ on the surface, the initial surface configuration is $(CO_2\text{-}O_{surf})$-$(5Ag)_{surf}$ $(1Cu4Ag)_{sub}$, which then evolves along two reaction pathways:

(1) $O{=}CO_2^{\delta-}$ forms directly on $(5Ag)_{surf}$ $(1Cu4Ag)_{sub}$ with $\Delta G = -0.28$ eV; and

(2) Surface O attracts one Cu atom from the subsurface to substitute for one surface Ag atom with $\Delta G = -0.45$ eV, and then the surface O reacts with $CO_2$ to form $O{=}CO_2^{\delta-}$ on $(4Ag1Cu)_{surf}$ $(5Ag)_{sub}$ with $\Delta G = -0.08$ eV.

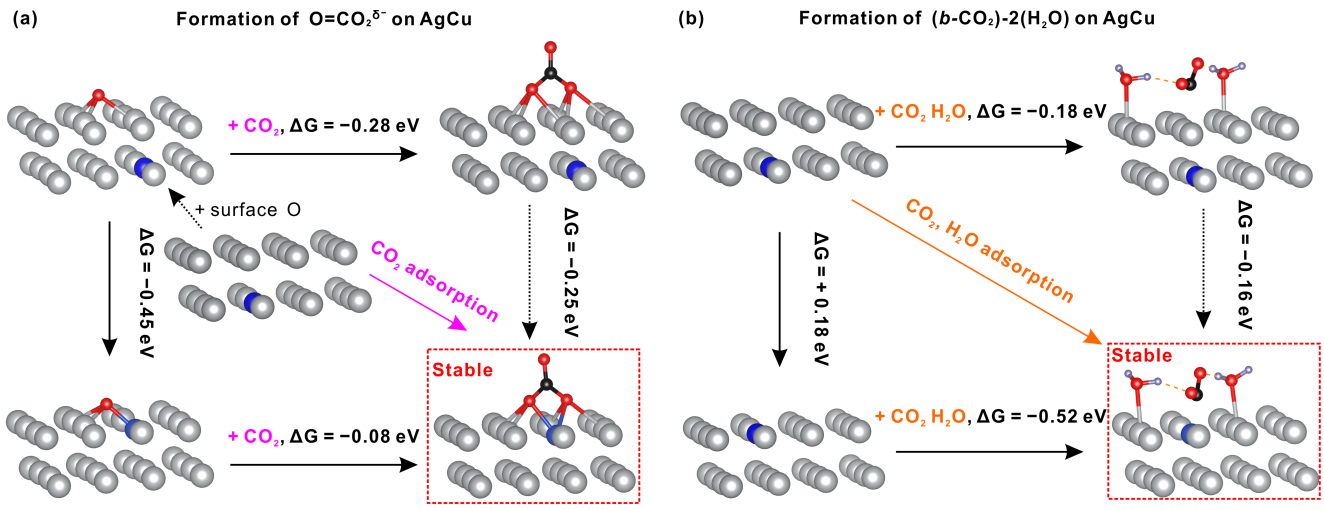


**Figure 2. The overall energy landscape of adsorbate formation on the AgCu surface with $CO_2$ adsorption alone and in the presence of $H_2O$ at 298 K. (a)** The formation of $O{=}CO_2^{\delta-}$ on AgCu surface. Starting with only Ag atoms as the first layer, surface O brings Cu to the surface to form the AgCu matrix, ΔG=−0.45 eV. Considering both chemistry driven surface reconstruction and adsorbate stability, we find that $O{=}CO_2^{\delta-}$ on 4Ag1Cu matrix is 0.25 eV more stable than on 5Ag. **(b)** The formation of ($b$-$CO_2$)-($H_2O$)$_2$ on the AgCu surface. When co-dosing $H_2O$ and $CO_2$, the most stable end result would be ($b$-$CO_2$)-($H_2O$)$_2$ on $(7Ag1Cu)_{surf}(8Ag)_{sub}$. We found that adsorption of $b$-$CO_2$ with $H_2O$ under experimental condition has a ΔG=−0.52 eV. Considering both chemistry driven surface reconstruction and adsorbate stability, we found that ($b$-$CO_2$)-($H_2O$)$_2$ on $(7Ag1Cu)_{surf}(8Ag)_{sub}$ is 0.16 eV more stable than on $8(Ag)_{surf}(7Ag1Cu)_{sub}$.

Considering that surface O prefers by 0.45 eV to adsorb on a Cu site rather than an Ag site (**Figure S2**), reaction pathway (2) has a relative free energy of (−0.45) + (−0.08) − (−0.28) = −0.25 eV compared to reaction pathway (1) (**Figure 2a**). Thus, case (2) with formation of $O{=}CO_2^{\delta-}$ on the AgCu surface having 4Ag and 1Cu is energetically more favorable by 0.25 eV than case (1) with formation of $O{=}CO_2^{\delta-}$ on AgCu surface having 5Ag sites.

Similarly, ($b$-$CO_2$)-($H_2O$)$_2$ on AgCu is only stable when one subsurface Cu atom substitutes for one surface Ag atom (**Figure 2b**). We considered the changes of the top two layers and the eight atoms that interact closely with ($b$-$CO_2$)-($H_2O$)$_2$ (**Figure 1d,** and **Figure S**5). We find that ($b$-$CO_2$)-($H_2O$)$_2$ lands on $(8Ag)_{surf}$ $(1Cu7Ag)_{sub}$ with a ΔG = −0.18 eV, however, this also draws one subsurface Cu to the surface, with ΔG= −0.18 eV to form a more stable configuration: ($b$-$CO_2$)-($H_2O$)$_2$ on $(7Ag1Cu)_{surf}$ $(8Ag)_{sub}$ with ΔG= −0.52 eV. This process has a total free energy of (−0.52) − (−0.18) − (−0.18) = −0.16 eV (**Figure 2b**), leading to the ($b$-$CO_2$)-($H_2O$)$_2$ on $(7Ag1Cu)_{surf}$ $(8Ag)_{sub}$ the stable configuration.

The chemistry driven surface reconstruction is validated experimentally by the Ag 3d and Cu 3p spectroscopic intensity changes (**Figure 3, Figure S8**). The Ag 3d and Cu 3p signals were collected under photon energies of 670 eV and 380 eV to have the same depth profile. We find that after $CO_2$ adsorption on Ag-rich AgCu surface, the Cu 3p signal increased, while the Ag 3d signal decreased. This is due the migration of Cu to the surface and the signal attenuation from the adsorbate layer (**Figure 3a**). The increase of Cu 3p by 135.1% after $CO_2$ adsorption for the Ag-rich AgCu surface is a strong indicator of the surface reconstruction. On the contrary, the Cu signal decreases on the Ag-lean surface (**Figure S**8), mainly because of signal attenuation through the adsorbate layer. However, Cu migration is still observed as an increased Cu:Ag ratio after $CO_2$ adsorption (**Figure 3c**). A chemistry driven surface reconstruction process similar to that induced by $CO_2$ adsorption alone is also observed when the surface is exposed to $CO_2$ in the presence of $H_2O$ (**Figure 3b**). We found that Cu migration occurs on both Ag-lean and Ag-rich surfaces, showing as Cu:Ag ratio increment, but it is more obvious on the Ag-rich surface (**Figure 3c**).

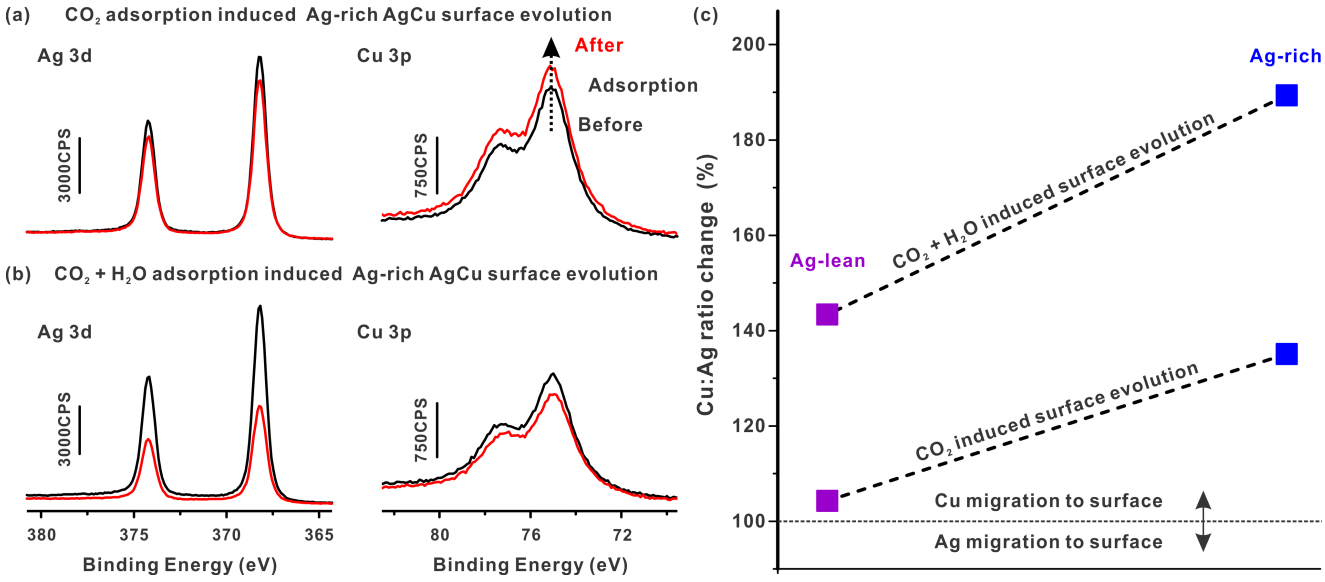


**Figure 3. The changes of catalysts component distribution induced by the gas adsorption.** The Ag 3d and Cu 3p intensity changes because of the $CO_2$ adsorption **(a)** alone and **(b)** in the presence of $H_2O$. **(c)** The Cu:Ag ratio changes for Ag-lean and Ag-rich surfaces induced by the gas adsorption. With $CO_2$ adsorption, the Ag 3d signals decreased to 93.3% and 87.2%, while the Cu 3p signals changed to 97.3% and 135.1%, respectively, for Ag-lean and Ag-rich AgCu surfaces. With $CO_2$ and $H_2O$ co-adsorption, the Ag 3d signals decreased to 56.4% and 49.3%, while the Cu 3p signals decreased to 80.9% and 93.2%, respectively, for Ag-lean and Ag-rich AgCu surfaces. The catalyst signals did not show the same attenuation level after gas adsorption, indicating the surface reconstruction induced by the gas adsorption. The Cu:Ag ration change is higher than 100% for all the cases, proving the Cu migration to the surface induced by gas adsorption. The adsorption induced Cu migration is more obvious on the Ag-rich surface than on Ag-lean surface.

This surface reconstruction is correlated with the formation of surface O, which is probably formed by $CO_2$ or $H_2O$ dissociation on Ag sites. The surface O induced surface reconstruction has been well established on Ag (111) and Cu (111) surfaces.[43-44] Our previous works showed that the adsorption of $CO_2$ is not stable on Ag (111) surface with Ag vacancy induced by surface O,[24] and $CO_2$ is also not stable on the oxygen covered Cu (111) surface.[22] Thus, we consider that $CO_2$ dissociates at the Ag site to form CO and surface O that further attracts subsurface or bulk Cu to initiate surface reconstruction. The surface O is observed as a ~529.8 eV peak in the O 1s spectra on both surfaces exposed to $CO_2$ (and $H_2O$), corresponding to the $O_{ads}$ on Cu (**Figure S9**). Thus, the configuration of (O-Cu)-Ag formed with surface O adsorption. However, this configuration shows different properties with the previously extensively reported Cu-metal oxide system.[25-26, 29-30] The Cu atoms interacting with $O_{ads}$ would not provide sites for $CO_2$ adsorption.[22] Instead, the Cu atoms interacting with Ag atoms can initiate the $CO_2$ adsorption (**Figure 1** and **Figure S6**). This configuration (Figure 1a,b) behaved like Ag-$O_x$-Cu interface, where the surface O and Cu tuned the $CO_2$ adsorption on the Ag site (**Figure 2a**). The Ag-rich surface has more Ag sites interacting with Cu compared with the Ag-lean surface, allowing more surface O formation to initiate Cu migration (**Figure 3c**), which also in turn changes the adsorbate-catalyst interactions. The surface reconstruction process shows a synergetic effect between Ag and Cu that tunes the $CO_2$ adsorption. We further investigated the $CO_2$ adsorption on the oxidized AgCu surface. The AgCu surface was heated in 30 mTorr $O_2$ at 450 K for 5mins. We found that Ag 3d intensity decreased significantly, while the Cu 3p intensity increased (**Figure S10**). Moreover, we observed an O 1s peak locating at 530.3 eV after AgCu treated in $O_2$, representing the formation the $CuO_x$ ($Cu_2O$ dominated). Thus, we concluded that heating AgCu in 30 mTorr $O_2$ at 450 K leads to the formation of a $CuO_x$ layer on top of AgCu, denoting as $CuO_xAg$. $CO_2$ adsorption on this $CuO_xAg$ surface leads to a peak appearing at around 289 eV, corresponding to the ionic carbonate, which is in line with previous study.[22]

Our studies lead to new insights about $CO_2$ adsorption on the AgCu bimetallic surface. Unlike on pure metal surfaces, gas adsorption on the bimetallic surface depends on the energetics of chemistry driven surface reconstruction in addition to the surface adsorbate stability. The $CO_2$-AgCu interactions change as the surface evolves, showing tunability of $CO_2$ adsorption on AgCu. Surface reconstruction for bimetallic systems induced by gas adsorption is well-known[45-50], but the atomic level detail have not been available. We find that the surface reconstruction induced by gas adsorption changes the underlying energetics of surface adsorbates. The synergetic effect between the Ag and Cu modifies the interactions between adsorbates and catalyst by changing the active surface sites and adsorption configurations. These results provide fresh insights into $CO_2$ adsorption and the initial steps of $CO_2$ activation on AgCu surfaces, showing surface reconstruction that is dramatically different from the pure Ag and Cu surfaces.

## 4. Conclusions

Our study emphasizes the power of combining advanced surface characterization techniques, APXPS, with QM predictions to provide a new level of atomistic understanding of how surface phenomena modify the fundamental underlying $CO_2$ adsorption and activation on bimetallic surface. We discovered how the $CO_2$ adsorption on AgCu bimetallic surface is tuned by the synergy between Ag and Cu. We find that the energetics of chemistry driven surface reconstruction can significantly modify the surface adsorbates properties, providing a new insight for manipulating the alloy surface to achieve selectivity and activity. These findings should stimulate new thinking about $CO_2$ reduction reactions on bimetallic surfaces, suggesting that the stabilization and activation of various adsorption configurations can be controlled through alloying different metals and suitable surface modifications.

## ASSOCIATED CONTENT

The Supporting Information is available free of charge on the ACS Publications website.

**Supplementary Information Contents**:

**Computational Methods**

**Table S1:** Convergence test with Ag substrates of 4-7 layers.

**Table S2:** Stability of $O{=}CO_2^{\delta-}$ on pure Ag and pure Ag unit with one Ag replaced by Cu at the first layer, second layer and third layer.

**Figure S1:** Catalyst component distribution of Ag-lean and Ag-rich AgCu surfaces before gas adsorption.

**Figure S2:** The driven force for AgCu surface reconstruction.

**Figure S3:** Catalyst component distribution change driven by thermal treatment under vacuum and with $O_2$.

**Figure S4:** Surface O can attract up to 3 atoms from subsurface to surface.

**Figure S5:** Topview for stable adsorbates on AgCu surface.

**Figure S6:** Configurations of interests for adsorbates on AgCu surface.

**Figure S7:** Comparisons of $CO_2$ adsorption on Ag, Cu, and AgCu surfaces characterized by C 1s APXPS.

**Figure S8:** Ag 3d and Cu 3p intensity changes after $CO_2$ adsorption both alone and in the presence of $H_2O$**.**

**Figure S9:** O 1s APXPS recorded on AgCu surface after $CO_2$ adsorption both alone and in the presence of $H_2O$.

**Figure S10:** APXPS recorded on $O_2$ treated AgCu surface before and after $CO_2$ adsorption.

## Authors Information

**Corresponding Author:**

*jyano@lbl.gov (J.Y.).

*wag@caltech.edu (W.A.G.).

*ejcrumlin@lbl.gov (E.J.C.).

**ORCID:**

Yifan Ye: 0000-0002-9393-0543

Jin Qian: 0000-0002-0162-0477

Hao Yang: 0000-0002-8241-6231

Tao Cheng: 0000-0003-4830-177X

Junko Yano: 0000-0001-6308-9071

Ethan J. Crumlin: 0000-0003-3132-190X

William A. Goddard, III: 0000-0003-0097-5716

**Author Contributions:**

#Y.Y., J.Q. and H.Y. contributed equally.

**Competing interests:**

The authors declare no competing interests.

**Acknowledgements**:

This work was supported through the Office of Science, Office of Basic Energy Science (BES), of the US Department of Energy (DOE) under Award DE-SC0004993 to the Joint Center for Artificial Photosynthesis, DOE Energy Innovation Hubs. The Advanced Light Source is supported by the Director, Office of Science, Office of BES, of the US DOE under Contract DE-AC02-05CH11231.

H.Y. and H.S. gratefully acknowledge China Scholarship Council (CSC, No. 201608320161 and No. 201706340112) for financial support.

This work used the Extreme Science and Engineering Discovery Environment (XSEDE), which is supported by National Science Foundation grant number ACI-1548562.

Y.Y., J.Q., and E.J.C. were partially supported by an Early Career Award in the Condensed Phase and Interfacial Molecular Science Program, in the Chemical Sciences Geosciences and Biosciences Division of the Office of Basic Energy Sciences of the U.S. Department of Energy under Contract No. DE-AC02-05CH11231.

T.C. and H.Y. thank the financial supports by the National Natural Science Foundation of China (21975148), the Natural Science Foundation of Jiangsu Higher Education Institutions (SBK20190810), and Jiangsu Province High-Level Talents (JNHB-106), the Priority Academic Program Development of Jiangsu Higher Education Institutions (PAPD). T.C. and H.Y. are supported by grants from startup supports of Soochow University and the Program for Jiangsu Specially-Appointed Professors to T.C.. H.Y. thanks China Postdoctoral Science Foundation (2019M660128) for financial support. This work was partly supported by Collaborative Innovation Center of Suzhou Nano Science & Technology.

**References:**

(1) Gao, S.; Lin, Y.; Jiao, X.; Sun, Y.; Luo, Q.; Zhang, W.; Li, D.; Yang, J.; Xie, Y. Partially oxidized atomic cobalt layers for carbon dioxide electroreduction to liquid fuel. *Nature* **2016,** *529* (7584), 68-71, DOI: 10.1038/nature16455.

(2) Liu, M.; Pang, Y.; Zhang, B.; De Luna, P.; Voznyy, O.; Xu, J.; Zheng, X.; Dinh, C. T.; Fan, F.; Cao, C.; de Arquer, F. P. G.; Safaei, T. S.; Mepham, A.; Klinkova, A.; Kumacheva, E.; Filleter, T.; Sinton, D.; Kelley, S. O.; Sargent, E. H. Enhanced electrocatalytic $CO_2$ reduction via field-induced reagent concentration. *Nature* **2016,** *537* (7620), 382-386, DOI: 10.1038/nature19060.

(3) Jinghua, W.; Yang, H.; Wen, Y.; Yanguang, L. $CO_2$ reduction: From the electrochemical to photochemical approach. *Adv. Sci.* **2017,** *4* (11), 1700194, DOI: doi:10.1002/advs.201700194.

(4) Yang, H. B.; Hung, S.-F.; Liu, S.; Yuan, K.; Miao, S.; Zhang, L.; Huang, X.; Wang, H.-Y.; Cai, W.; Chen, R.; Gao, J.; Yang, X.; Chen, W.; Huang, Y.; Chen, H. M.; Li, C. M.; Zhang, T.; Liu, B. Atomically dispersed Ni(i) as the active site for electrochemical $CO_2$ reduction. *Nat. Energy* **2018,** *3* (2), 140-147, DOI: 10.1038/s41560-017-0078-8.

(5) Chu, S.; Majumdar, A. Opportunities and challenges for a sustainable energy future. *Nature* **2012,** *488* (7411), 294-303, DOI: 10.1038/nature11475.

(6) Appel, A. M.; Bercaw, J. E.; Bocarsly, A. B.; Dobbek, H.; DuBois, D. L.; Dupuis, M.; Ferry, J. G.; Fujita, E.; Hille, R.; Kenis, P. J. A.; Kerfeld, C. A.; Morris, R. H.; Peden, C. H. F.; Portis, A. R.; Ragsdale, S. W.; Rauchfuss, T. B.;

Reek, J. N. H.; Seefeldt, L. C.; Thauer, R. K.; Waldrop, G. L. Frontiers, opportunities, and challenges in biochemical and chemical catalysis of $CO_2$ fixation. *Chem. Rev.* **2013,** *113* (8), 6621-6658, DOI: 10.1021/cr300463y.
(7) Bagger, A.; Ju, W.; Varela, A. S.; Strasser, P.; Rossmeisl, J. Electrochemical $CO_2$ reduction: A classification problem. *ChemPhysChem* **2017,** *18* (22), 3266-3273, DOI: 10.1002/cphc.201700736.
(8) Hoshi, N.; Kato, M.; Hori, Y. Electrochemical reduction of $CO_2$ on single crystal electrodes of silver Ag(111), Ag(100) and Ag(110). *J. Electroanal. Chem.* **1997,** *440* (1), 283-286, DOI: https://doi.org/10.1016/S0022-0728(97)00447-6.
(9) Back, S.; Yeom, M. S.; Jung, Y. Understanding the effects of Au morphology on $CO_2$ electrocatalysis. *J. Phys. Chem. C* **2018,** *122* (8), 4274-4280, DOI: 10.1021/acs.jpcc.7b10439.
(10) Zhuang, T.-T.; Liang, Z.-Q.; Seifitokaldani, A.; Li, Y.; De Luna, P.; Burdyny, T.; Che, F.; Meng, F.; Min, Y.; Quintero-Bermudez, R.; Dinh, C. T.; Pang, Y.; Zhong, M.; Zhang, B.; Li, J.; Chen, P.-N.; Zheng, X.-L.; Liang, H.; Ge, W.-N.; Ye, B.-J.; Sinton, D.; Yu, S.-H.; Sargent, E. H. Steering post-C–C coupling selectivity enables high efficiency electroreduction of carbon dioxide to multi-carbon alcohols. *Nat. Catal.* **2018,** *1* (6), 421-428, DOI: 10.1038/s41929-018-0084-7.
(11) Hemma, M.; Yong-Wook, C.; Alexander, B.; Fabian, S.; S., B. C.; Ilya, S.; J., D. N.; Ioannis, Z.; Sang, J. H.; Kim, K.; A., S. E.; C., Y. J.; Jan, R.; Beatriz, R. C. Enhanced carbon dioxide electroreduction to carbon monoxide over defect-rich plasma-activated silver catalysts. *Angew. Chem. Int. Ed.* **2017,** *129* (38), 11552-11556, DOI: doi:10.1002/ange.201704613.
(12) Chen, Y.; Li, C. W.; Kanan, M. W. Aqueous $CO_2$ reduction at very low overpotential on oxide-derived Au nanoparticles. *J. Am. Chem. Soc.* **2012,** *134* (49), 19969-19972, DOI: 10.1021/ja309317u.
(13) Mistry, H.; Varela, A. S.; Bonifacio, C. S.; Zegkinoglou, I.; Sinev, I.; Choi, Y.-W.; Kisslinger, K.; Stach, E. A.; Yang, J. C.; Strasser, P.; Cuenya, B. R. Highly selective plasma-activated copper catalysts for carbon dioxide reduction to ethylene. *Nat. Commun.* **2016,** *7* (1), 12123, DOI: 10.1038/ncomms12123.
(14) Schouten, K. J. P.; Kwon, Y.; van der Ham, C. J. M.; Qin, Z.; Koper, M. T. M. A new mechanism for the selectivity to $C_1$ and $C_2$ species in the electrochemical reduction of carbon dioxide on copper electrodes. *Chem. Sci.* **2011,** *2* (10), 1902-1909, DOI: 10.1039/C1SC00277E.
(15) Hori, Y.; Takahashi, I.; Koga, O.; Hoshi, N. Selective formation of $C_2$ compounds from electrochemical reduction of $CO_2$ at a series of copper single crystal electrodes. *J. Phys. Chem. B* **2002,** *106* (1), 15-17, DOI: 10.1021/jp013478d.
(16) Kim, D.; Kley, C. S.; Li, Y.; Yang, P. Copper nanoparticle ensembles for selective electroreduction of $CO_2$ to $C_2$–$C_3$ products. *Proc. Natl. Acad. Sci. USA* **2017,** *114* (40), 10560-10565, DOI: 10.1073/pnas.1711493114.
(17) Kim, D.; Resasco, J.; Yu, Y.; Asiri, A. M.; Yang, P. Synergistic geometric and electronic effects for electrochemical reduction of carbon dioxide using gold–copper bimetallic nanoparticles. *Nat. Commun.* **2014,** *5* (1), 4948, DOI: 10.1038/ncomms5948.
(18) Chang, Z.; Huo, S.; Zhang, W.; Fang, J.; Wang, H. The tunable and highly selective reduction products on Ag@Cu bimetallic catalysts toward $CO_2$ electrochemical reduction reaction. *J. Phys. Chem. C* **2017,** *121* (21), 11368-11379, DOI: 10.1021/acs.jpcc.7b01586.
(19) Kottakkat, T.; Klingan, K.; Jiang, S.; Jovanov, Z. P.; Davies, V. H.; El-Nagar, G. A. M.; Dau, H.; Roth, C. Electrodeposited AgCu foam catalysts for enhanced reduction of $CO_2$ to CO. *ACS Appl. Mate. Interfaces* **2019,** *11* (16), 14734-14744, DOI: 10.1021/acsami.8b22071.
(20) Huang, J.; Mensi, M.; Oveisi, E.; Mantella, V.; Buonsanti, R. Structural sensitivities in bimetallic catalysts for electrochemical $CO_2$ reduction revealed by Ag–Cu nanodimers. *J. Am. Chem. Soc.* **2019,** *141* (6), 2490-2499, DOI: 10.1021/jacs.8b12381.
(21) Clark, E. L.; Hahn, C.; Jaramillo, T. F.; Bell, A. T. Electrochemical $CO_2$ reduction over compressively strained CuAg surface alloys with enhanced multi-carbon oxygenate selectivity. *J. Am. Chem. Soc.* **2017,** *139* (44), 15848-15857, DOI: 10.1021/jacs.7b08607.
(22) Favaro, M.; Xiao, H.; Cheng, T.; Goddard, W. A.; Yano, J.; Crumlin, E. J. Subsurface oxide plays a critical role in $CO_2$ activation by Cu(111) surfaces to form chemisorbed $CO_2$, the first step in reduction of $CO_2$. *Proc. Natl. Acad. Sci. USA* **2017,** *114* (26), 6706-6711, DOI: 10.1073/pnas.1701405114.
(23) Xiao, H.; Goddard, W. A.; Cheng, T.; Liu, Y. Cu metal embedded in oxidized matrix catalyst to promote $CO_2$ activation and CO dimerization for electrochemical reduction of $CO_2$. *Proc. Natl. Acad. Sci. USA* **2017,** *114* (26), 6685-6688, DOI: 10.1073/pnas.1702405114.
(24) Ye, Y.; Yang, H.; Qian, J.; Su, H.; Lee, K.-J.; Cheng, T.; Xiao, H.; Yano, J.; Goddard, W. A.; Crumlin, E. J. Dramatic differences in carbon dioxide adsorption and initial steps of reduction between silver and copper. *Nat. Commun.* **2019,** *10* (1), 1875, DOI: 10.1038/s41467-019-09846-y.
(25) Palomino, R. M.; Ramírez, P. J.; Liu, Z.; Hamlyn, R.; Waluyo, I.; Mahapatra, M.; Orozco, I.; Hunt, A.; Simonovis, J. P.; Senanayake, S. D.; Rodriguez, J. A. Hydrogenation of $CO_2$ on ZnO/Cu(100) and ZnO/Cu(111) catalysts: Role

of copper structure and metal–oxide interface in methanol synthesis. *J. Phys. Chem. B* **2018,** *122* (2), 794-800, DOI: 10.1021/acs.jpcb.7b06901.
(26) Rodriguez, J. A.; Liu, P.; Graciani, J.; Senanayake, S. D.; Grinter, D. C.; Stacchiola, D.; Hrbek, J.; Fernández-Sanz, J. Inverse oxide/metal catalysts in fundamental studies and practical applications: a perspective of recent developments. *J. Phys. Chem. Lett.* **2016,** *7* (13), 2627-2639, DOI: 10.1021/acs.jpclett.6b00499.
(27) Kattel, S.; Liu, P.; Chen, J. G. Tuning selectivity of $CO_2$ hydrogenation reactions at the metal/oxide interface. *J. Am. Chem. Soc.* **2017,** *139* (29), 9739-9754, DOI: 10.1021/jacs.7b05362.
(28) Orozco, I.; Huang, E.; Gutiérrez, R. A.; Liu, Z.; Zhang, F.; Mahapatra, M.; Kang, J.; Kersell, H.; Nemsak, S.; Ramírez, P. J.; Senanayake, S. D.; Liu, P.; Rodriguez, J. A. Hydroxylation of ZnO/Cu(1 1 1) inverse catalysts under ambient water vapor and the water–gas shift reaction. *J. Phys. D: Appl. Phys.* **2019,** *52* (45), 454001, DOI: 10.1088/1361-6463/ab37da.
(29) Hamlyn, R.; Mahapatra, M.; Orozco, I.; Hunt, A.; Waluyo, I.; White, M. G.; Senanayake, S. D.; Rodriguez, J. Morphology and chemical behavior of model CsOx/$Cu_2O$/Cu(111) nanocatalysts for methanol synthesis: Reaction with $CO_2$ and $H_2$. *J. Chem. Phys.* **2020,** *152* (4), 044701, DOI: 10.1063/1.5129152.
(30) Senanayake, S. D.; Ramírez, P. J.; Waluyo, I.; Kundu, S.; Mudiyanselage, K.; Liu, Z.; Liu, Z.; Axnanda, S.; Stacchiola, D. J.; Evans, J.; Rodriguez, J. A. Hydrogenation of $CO_2$ to methanol on CeOx/Cu(111) and ZnO/Cu(111) catalysts: role of the metal–oxide interface and importance of $Ce^{3+}$ sites. *J. Phys. Chem. C* **2016,** *120* (3), 1778-1784, DOI: 10.1021/acs.jpcc.5b12012.
(31) Rodriguez, J. A.; Grinter, D. C.; Liu, Z.; Palomino, R. M.; Senanayake, S. D. Ceria-based model catalysts: fundamental studies on the importance of the metal–ceria interface in CO oxidation, the water–gas shift, $CO_2$ hydrogenation, and methane and alcohol reforming. *Chem. Soc. Rev.* **2017,** *46* (7), 1824-1841, DOI: 10.1039/C6CS00863A.
(32) Grass, M. E.; Karlsson, P. G.; Aksoy, F.; Lundqvist, M.; Wannberg, B.; Mun, B. S.; Hussain, Z.; Liu, Z. New Ambient Pressure Photoemission Endstation at Advanced Light Source Beamline 9.3.2. *Rev. Sci. Instrum.* **2010,** *81* (5), 053106, DOI: 10.1063/1.3427218.
(33) Kresse, G.; Furthmüller, J. Efficient iterative schemes for ab initio total-energy calculations using a plane-wave basis set. *Phys. Rev. B* **1996,** *54* (16), 11169-11186, DOI: 10.1103/PhysRevB.54.11169.
(34) Grimme, S.; Antony, J.; Ehrlich, S.; Krieg, H. A consistent and accurate ab initio parametrization of density functional dispersion correction (DFT-D) for the 94 elements H-Pu. *J. Chem. Phys.* **2010,** *132* (15), 154104, DOI: 10.1063/1.3382344.
(35) Perdew, J. P.; Chevary, J. A.; Vosko, S. H.; Jackson, K. A.; Pederson, M. R.; Singh, D. J.; Fiolhais, C. Atoms, molecules, solids, and surfaces: Applications of the generalized gradient approximation for exchange and correlation. *Phys. Rev. B* **1992,** *46* (11), 6671-6687, DOI: 10.1103/PhysRevB.46.6671.
(36) Perdew, J. P.; Burke, K.; Ernzerhof, M. Generalized gradient approximation made simple. *Phys. Rev. Lett.* **1996,** *77* (18), 3865-3868, DOI: 10.1103/PhysRevLett.77.3865.
(37) Paxton, A. T.; Methfessel, M.; Polatoglou, H. M. Structural energy-volume relations in first-row transition metals. *Phys. Rev. B* **1990,** *41* (12), 8127-8138, DOI: 10.1103/PhysRevB.41.8127.
(38) Strohmeier, B. R. Copper/Silver/Gold Alloy by XPS. *Surf. Sci. Spectra* **1994,** *3* (3), 175-181, DOI: 10.1116/1.1247744.
(39) Aqra, F.; Ayyad, A. Surface energies of metals in both liquid and solid states. *Appl. Surf. Sci.* **2011,** *257* (15), 6372-6379, DOI: https://doi.org/10.1016/j.apsusc.2011.01.123.
(40) Henkelman, G.; Arnaldsson, A.; Jónsson, H. A fast and robust algorithm for Bader decomposition of charge density. *Comput. Mater. Sci.* **2006,** *36* (3), 354-360, DOI: https://doi.org/10.1016/j.commatsci.2005.04.010.
(41) Sanville, E.; Kenny, S. D.; Smith, R.; Henkelman, G. Improved grid-based algorithm for Bader charge allocation. *J. Comput. Chem.* **2007,** *28* (5), 899-908, DOI: doi:10.1002/jcc.20575.
(42) Xiao, H.; Cheng, T.; Goddard, W. A. Atomistic mechanisms underlying selectivities in $C_1$ and $C_2$ products from electrochemical reduction of CO on Cu(111). *J. Am. Chem. Soc.* **2017,** *139* (1), 130-136, DOI: 10.1021/jacs.6b06846.
(43) Niehus, H. Surface reconstruction of Cu (111) upon oxygen adsorption. *Surf. Sci.* **1983,** *130* (1), 41-49, DOI: https://doi.org/10.1016/0039-6028(83)90258-3.
(44) Andryushechkin, B. V.; Shevlyuga, V. M.; Pavlova, T. V.; Zhidomirov, G. M.; Eltsov, K. N. Adsorption of $O_2$ on Ag(111): Evidence of local oxide formation. *Phys. Rev. Lett.* **2016,** *117* (5), 056101, DOI: 10.1103/PhysRevLett.117.056101.
(45) Wu, C. H.; Liu, C.; Su, D.; Xin, H. L.; Fang, H.-T.; Eren, B.; Zhang, S.; Murray, C. B.; Salmeron, M. B. Bimetallic synergy in cobalt–palladium nanocatalysts for CO oxidation. *Nat. Catal.* **2019,** *2* (1), 78-85, DOI: 10.1038/s41929-019-0233-7.

(46) Eren, B.; Torres, D.; Karslıoğlu, O.; Liu, Z.; Wu, C. H.; Stacchiola, D.; Bluhm, H.; Somorjai, G. A.; Salmeron, M. Structure of copper–cobalt surface alloys in equilibrium with carbon monoxide gas. *J. Am. Chem. Soc.* **2018,** *140* (21), 6575-6581, DOI: 10.1021/jacs.7b13621.
(47) Eren, B.; Zherebetskyy, D.; Patera, L. L.; Wu, C. H.; Bluhm, H.; Africh, C.; Wang, L.-W.; Somorjai, G. A.; Salmeron, M. Activation of Cu(111) surface by decomposition into nanoclusters driven by CO adsorption. *Science* **2016,** *351* (6272), 475-478, DOI: 10.1126/science.aad8868.
(48) Tao, F.; Grass, M. E.; Zhang, Y.; Butcher, D. R.; Renzas, J. R.; Liu, Z.; Chung, J. Y.; Mun, B. S.; Salmeron, M.; Somorjai, G. A. Reaction-driven restructuring of Rh-Pd and Pt-Pd core-shell nanoparticles. *Science* **2008,** *322* (5903), 932-934, DOI: 10.1126/science.1164170.
(49) Tao, F.; Grass, M. E.; Zhang, Y.; Butcher, D. R.; Aksoy, F.; Aloni, S.; Altoe, V.; Alayoglu, S.; Renzas, J. R.; Tsung, C.-K.; Zhu, Z.; Liu, Z.; Salmeron, M.; Somorjai, G. A. Evolution of structure and chemistry of bimetallic nanoparticle catalysts under reaction conditions. *J. Am. Chem. Soc.* **2010,** *132* (25), 8697-8703, DOI: 10.1021/ja101502t.
(50) Gauthier, Y.; Schmid, M.; Padovani, S.; Lundgren, E.; Buš, V.; Kresse, G.; Redinger, J.; Varga, P. Adsorption sites and ligand effect for CO on an alloy surface: A direct view. *Phys. Rev. Lett.* **2001,** *87* (3), 036103, DOI: 10.1103/PhysRevLett.87.036103.

**For Table of Contents Only**